Electronic State Spectroscopy of c-C_5F_8 Explored by Photoabsorption, Electron Impact, Photoelectron Spectroscopies and Ab Initio Calculations

P. Limão-Vieira,*,†,‡ D. Duflot,§ A. Giuliani,||,&,⊥ E. Vasekova,‡ J. M. C. Lourenço,† P. M. Santos,# S. V. Hoffmann,▽ N. J. Mason,‡ J. Delwiche,|| and M.-J. Hubin-Franskin||

Laboratório de Colisões Atómicas e Moleculares, Departamento de Física, CEFITEC, Universidade Nova de Lisboa, P-2829-516 Caparica, Portugal, Centre of Molecular and Optical Sciences, Department of Physics and Astronomy, The Open University, Walton Hall, Milton Keynes, MK7 6AA, U.K., Laboratoire de Physique des Lasers, Atomes et Molécules (PhLAM), UMR CNRS 8523, Centre d'Études et de Recherches Lasers et Applications (CERLA, FR CNRS 2416), Université des Sciences et Technologies de Lille, F-59655 Villeneuve d'Ascq Cedex, France, Laboratoire de Spectroscopie d'Électrons Diffusés, Université de Liège, Institut de Chimie-Bât. B6c B-4000 Liège 1, Belgium, DISCO Beamline, Synchrotron SOLEIL, BP 48, L'Orme des Merisiers, 91192 Gif-sur-Yvette CEDEX, France and Cepia, Institut National de la Recherche Agronomique, BP 71627, F-44316, France, Instituto de Telecomunicações, IST, Avenida Rovisco Pais, P-1049-001 Lisboa, Portugal, and Institute for Storage Ring Facilities, University of Aarhus, Ny Munkegade, DK-8000, Aarhus C, Denmark

Received: November 12, 2007

The electronic transitions and resonance-enhanced vibrational excitations of octafluorocyclopentene (c-C_5F_8) have been investigated using high-resolution photoabsorption spectroscopy in the energy range 6−11 eV. In addition, the high-resolution electron energy loss spectrum (HREELS) was recorded under the electric dipolar excitation conditions (100 eV incident energy, ∼0° scattering angle) over the 5−14 eV energy loss range. A He(I) photoelectron spectrum (PES) has also been recorded between 11 and 20 eV, allowing us to derive a more precise value of (11.288 ± 0.002) eV for the ground neutral state adiabatic ionization energy. All spectra presented in this paper represent the first and highest resolution data yet reported for octafluorocyclopentene. Ab initio calculations have been performed for helping in the assignment of the spectral bands for both neutral excited states and ionic states.

1. Introduction

As part of an international effort to reduce the emission of atmospheric pollutants that may lead to global warming the Kyoto Protocol and its amendments have been developed to phase out the use of several anthropogenic gases by 2010, including several species arising from the plasma processing industries. Therefore, in order to meet the requirements of the Kyoto Protocol, industry has been seeking alternative gases that will both operate in current plasma reactors and maintain high performance of current feed gases (e.g., SF_6 and CF_4). Octafluorocyclopentene, c-C_5F_8, is among the fluorocarbons suggested as a candidate to replace the traditional feed gases used in the semiconductor industry to prepare silicon wafers for SiO_2 reactive ion etching.[1] Surface reactions induced by c-C_5F_8 plasmas have been studied on silicon dioxide and silicon nitride substrates using an inductively coupled plasma source, revealing larger etching selectivity and polymerization than in a more conventional c-C_4F_8 plasma.[2] However, before c-C_5F_8 can be widely adopted it must be shown to have little (or no) environmental impact.

To compute the global warming potential (GWP) and lifetime of any atmospheric molecule, one requires both knowledge of the electronic state spectroscopy and the absolute photoabsorption cross-sectional values in the visible and vacuum ultraviolet (VUV) region of the electromagnetic spectrum.[3] As part of a larger project to investigate the electronic state spectroscopy of several plasma processing molecules and to evaluate their role in global warming in the earth's atmosphere (see, e.g., ref 4), we have, therefore, recorded high-resolution VUV photoabsorption, electron energy loss, and photoelectron spectra (PESs) of c-C_5F_8. As far as we are aware, no other spectra have been reported in the literature. Indeed, a review of the literature reveals little experimental data for c-C_5F_8, these being limited to some measurements of the electron attachment line shapes and cross sections at ultralow electron energies.[5] Recent studies on the ionization cross sections of Jiao et al.[6] on cation−molecule reactions and Parkes et al.[7] on threshold photoelectron−photoion coincidence spectroscopy with a He(I) PES obtained with a lower resolution that in the present work have been reported. Quantum chemical studies via configuration interaction scheme (CIS) with the Hartree−Fock method[8] and ab initio calculations on the dissociative attachment resonance energies with comparisons to electron attachment mass spectrometric measurements[9] have also been discussed in a recent

* Corresponding author. Mailing address: Laboratório de Colisões Atómicas e Moleculares, Departamento de Física, CEFITEC, Universidade Nova de Lisboa, P-2829-516 Caparica, Portugal. E-mail address: plimaovieira@fct.unl.pt. Tel: +351-21 294 85 76. Fax: + 351-21 294 85 49.

† Universidade Nova de Lisboa.
‡ The Open University.
§ Université des Sciences et Technologies de Lille.
|| Université de Liège.
& DISCO Beamline, Synchrotron SOLEIL.
⊥ Institut National de la Recherche Agronomique.
Instituto de Telecomunicações, IST.
▽ University of Aarhus.

10.1021/jp7107939 CCC: $40.75
Published on Web 03/11/2008

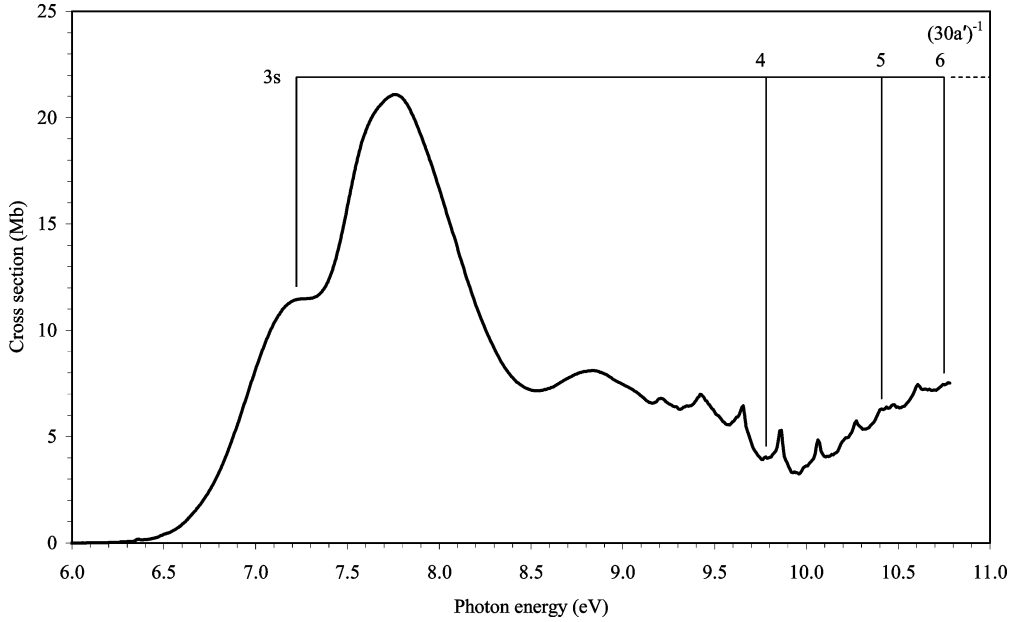

Figure 1. High-resolution VUV photoabsorption spectrum of c-C_5F_8, recorded using the Århus synchrotron facility, showing valence and Rydberg states in the 6−11 eV energy range.

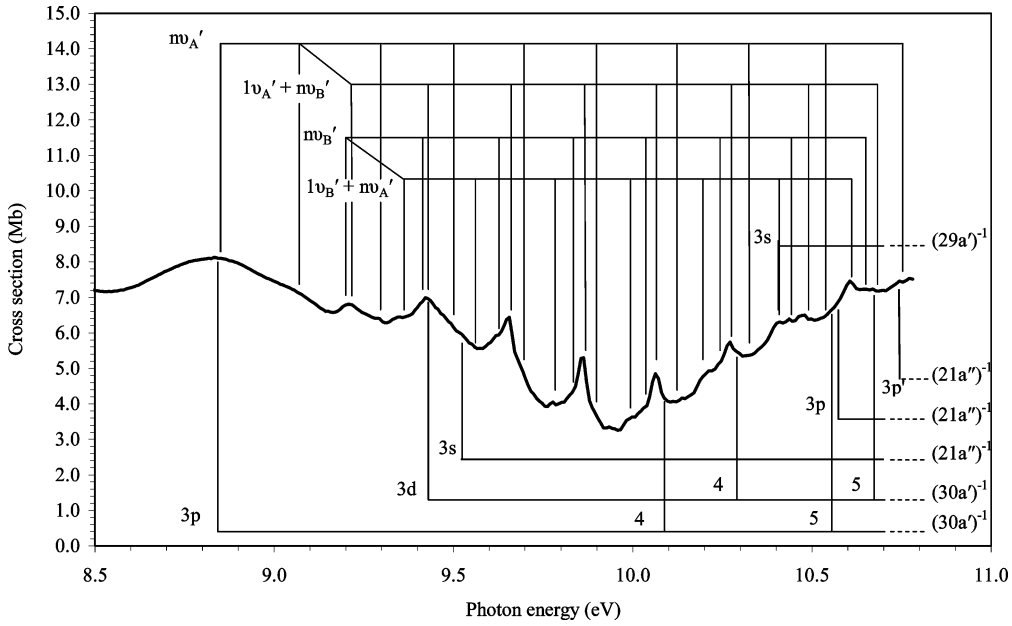

Figure 2. High-resolution VUV photoabsorption spectrum of c-C_5F_8, recorded using the Århus synchrotron radiation facility, showing valence and Rydberg states and vibrational progressions in the 8.5−11.0 eV energy range.

work, but the former has proven to disagree with our present calculations (see Computational Method section).

Electron energy loss spectra in the present experiments and excitation energies derived from theory are used to help assign the major bands in the photoabsorption spectra. Further information is derived from a high-resolution PES, which is used to help in the identification of Rydberg states in the VUV spectrum.

The VUV absolute photoabsorption cross section of c-C_5F_8 reported in this paper is used to derive its photolysis lifetime in the earth's atmosphere and compared to other candidates for replacement in the plasma industry.

2. Experimental Section

The electronic states of octafluorocyclopentene (c-C_5F_8) spectroscopy has been studied using a range of different experimental techniques, including (1) VUV photoabsorption using a synchrotron radiation source, which provides data on optical allowed transitions, (2) high-resolution electron energy loss spectroscopy (HREELS) in electric dipolar interaction conditions, which allow only optically allowed transitions to be monitored, and (3) He(I) photoelectron spectroscopy (PES) to determine the ionization energies. HREELS was used in order to increase the energy range studied, the VUV absorption curve being limited in energy by the transmission limit of the entrance window of the photoabsorption cell (see below).

2.1. VUV Photoabsorption. The high-resolution VUV photoabsorption measurements (Figures 1 and 2) were performed using the ASTRID−UV1 beam line at the Institute for Storage Ring Facilities (ISA), University of Aarhus, Denmark. A detailed description of the apparatus can be found elsewhere,[10] so only

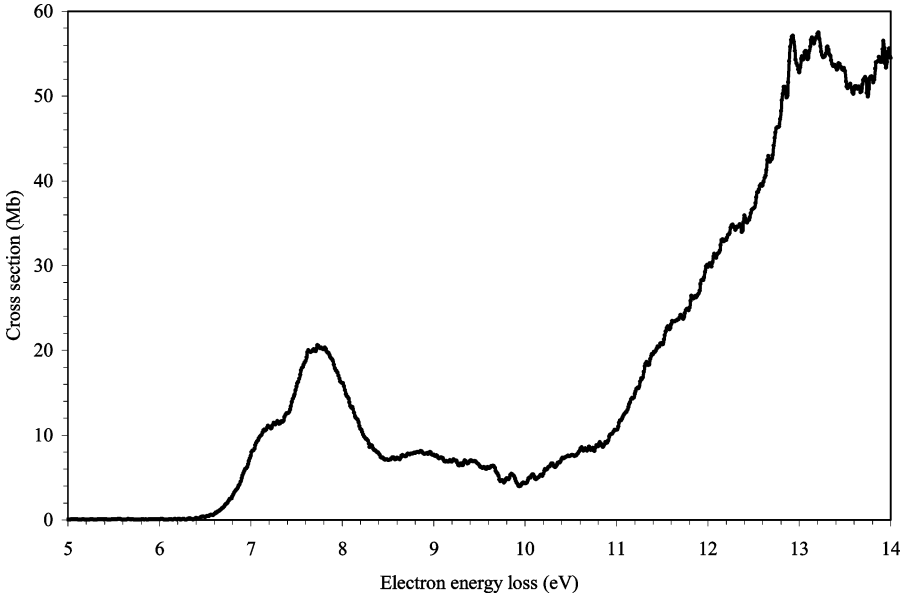

Figure 3. Electron energy loss spectrum of c-C_5F_8 recorded at the University of Liège in the 5−14 eV energy region in electric dipolar interaction conditions (100 eV incident energy, $\approx 0°$ scattering angle).

a brief description will be given here. A toroidal dispersion grating is used to select the synchrotron radiation with a full width at half-maximum (fwhm) wavelength resolution of approximately 0.075 nm. The synchrotron radiation passes through the static gas sample at room temperature. A photomultiplier is used to detect the transmitted light. For wavelengths below 200 nm, a flow of He gas is flushed through the small gap between the photomultiplier and the exit window of the gas cell to prevent any absorption by air contributing to the spectrum. A LiF entrance window acts as an edge filter for higher-order radiation, restricting the photoabsorption measures to below 10.8 eV (115 nm). The grating itself provides a maximum wavelength (lower energy limit) of 320 nm (3.9 eV). The sample pressure is measured by a Baratron capacitance gauge. To avoid any saturation effects, sample pressures were chosen such that the transmitted flux was >10% of the incident flux.

Gas transmission results are compared to a background scan recorded with an evacuated cell. Absolute photoabsorption cross sections may then be calculated using the Beer−Lambert law:

$$I_t = I_0 \exp(-n\sigma x)$$

where I_t is the intensity of the light transmitted through the gas sample, I_0 is that through the evacuated cell, n is the molecular number density of the sample gas, σ is the absolute photoabsorption cross section, and x is the absorption path length (25 cm). The accuracy of the absolute cross section is estimated to be better than ±5%.

2.2. High-Resolution Electron Energy Loss Spectroscopy. The instrument used at the Université de Liège, Belgium (VG-SEELS 400) has been described in detail elsewhere.[11] An electrostatic electron energy monochromator defines a narrow energy spread about the mean incident electron energy, and a three element lens focuses the electrons into the collision region. The electron beam intersects the effusive gas beam, which flows through a hypodermic needle, at 90°. The working pressure in the chamber with target gas is $\sim 1.5 \times 10^{-5}$ mbar. The analyzer system is also an electrostatic energy analyzer[12] with the scattered electron signal detected by an electron multiplier of the continuous dynode type. Both electron energy selectors work in the constant pass-energy mode. Spectra were recorded for energy losses between 5.0 and 14 eV at step intervals of 10 meV. The electron energy loss scale was calibrated to the "elastic scattering peak". The resolution, measured as the fwhm of the elastically scattered electron peak was about 40 meV. The apparatus was used with relatively high incident energy electrons (100 eV) and a quite small scattering angle ($\theta \approx 0°$), such that strictly electric dipole interaction conditions apply. The derived VUV cross section was normalized at 8.57 eV from our VUV photoabsorption value of 7.203 Mbar to obtain absolute cross section values, a method shown to be reliable in previous works (see, e.g., ref 12). Comparison of the HREELS cross section values with those recorded using the synchrotron radiation source thus provides a test for any systematic errors in the optical values arising from the line saturation effect and second-order light from the light source and beam line. These were found to be negligible in this work. The present HREELS spectrum is shown in Figure 3.

2.3. Photoelectron Spectroscopy. He(I) (21.22 eV) photoelectron spectra of c-C_5F_8 (Figure 4) were taken at the Université de Liège, Belgium. The apparatus has been described in detail previously.[13] Briefly, the spectrometer consists of a 180° cylindrical electrostatic analyzer with a mean radius of 5 cm. The analyzer is used in constant energy pass mode. The incident photons are produced by a D.C. discharge in a two-stage differentially pumped lamp. The energy scale was calibrated using argon lines using the values $^2P_{3/2} = 15.760$ eV and $^2P_{1/2} = 15.937$ eV),[14,15] and the resolution of the present spectrum is measured from the fwhm of the Ar peaks to be 20 meV, in presence of c-C_5F_8. The position of the first peak in the first electronic band of the c-C_5F_8 PES was determined by making use of a least-square fitting with a Gaussian curve. Repeated tests in our laboratory have shown that this procedure is not very sensitive to the choice of the limits used for the fitting, and so the uncertainty of the position of a peak maximum is more or less one energy interval between two successive experimental points, giving, in the case of the c-C_5F_8 PES, an uncertainty of ±0.002 eV. The same procedure was used for

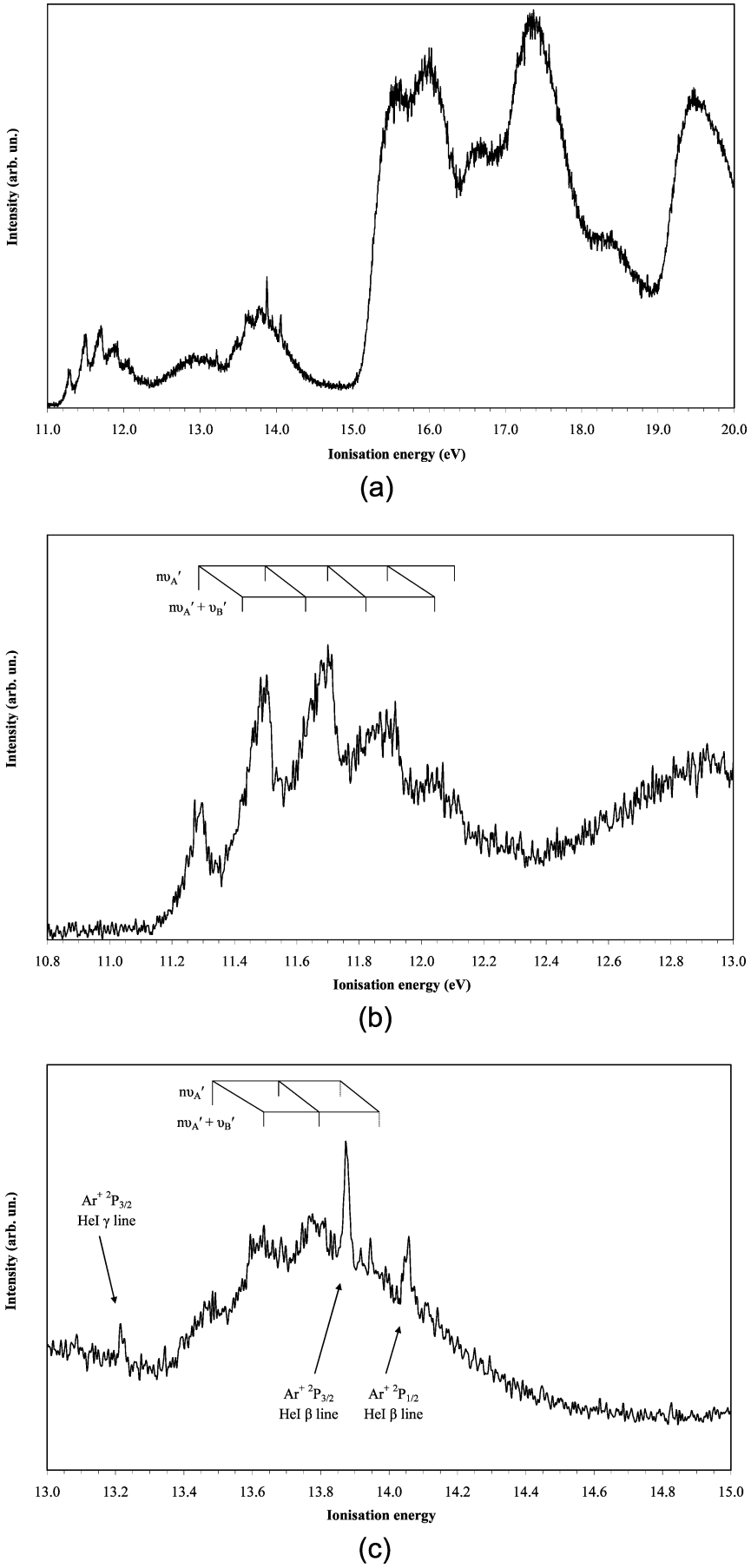

Figure 4. He(I) photoelectron spectra of c-C_5F_8 recorded at the University of Liège (a) in the 11−20 eV energy region, (b) in the 10.8−13.0 eV energy region, and (c) in the 13.0−15.0 eV energy region (see discussion in text).

all the energy values quoted in the paper. The intensities in the spectrum were corrected for the transmission of the analyzing system. The spectrum presented in Figure 4 consists of two parts, with the high-energy region (>15 eV) being recorded without Argon in order to avoid the strong signal due to the presence of the rare gas. The Ar lines shown in the lower energy part of the spectrum are due to Ar features produced by the He(I)β and γ lines, respectively. The PES presented in this paper is the sum of 22 individual spectra. This procedure allowed us to obtain a good signal-to-noise ratio while keeping the pressure in the spectrometer at a very low level ($<5 \times 10^{-6}$ mbar).

Octafluorocyclopentane Sample. The gas sample used in the VUV measurements was purchased from Fluorochem, with a minimum purity of 99%, while for PES and HREELS experiments, the sample was purchased from ABCR with a quoted 99.8% purity.

3. Computational Details

We performed ab initio calculations to determine vertical excitation energies of the electronic states and the lowest ionization energies. As recently reviewed,[16] the calculation of electronic spectra, especially for molecules with a large number of electrons, remains a difficult task. Because of its low computational cost, the time-dependent density functional theory (TDDFT) method has recently become a very popular method[16] and, in the case of the acrolein molecule, was shown to give results in good agreement with more costly calculations (i.e., MS-CASPT2), using the PBE0 functional.[17,18] Therefore, the same method was employed in the present work: the geometry of c-C_5F_8 was optimized at the DFT/PBE0/6-311G** level, and the electronic excitation spectrum was calculated at the TDDFT//PBE0/6-311++G** level. These calculations were performed with the Gaussian 03 package.[19] However, it is also well-known[16,20] that TDDFT has difficulties describing certain types of electronic states, such as Rydberg states. Thus, the lowest lying excited states of c-C_5F_8 were also computed at the EOM-CCSD[21] level with the MOLPRO program.[22] The geometry was optimized at the MP2/cc-pVDZ level with Gaussian, and then diffuse functions (5s, 5p, 5d) taken from Kaufmann et al.[23] were added at the center of the molecule (cc-pVDZ+R basis set). Finally, the lowest ionization energies of c-C_5F_8 were obtained with Gaussian at the UPBE0 level, and at the RCCSD[24] and RCCSD(T) levels[25] with MOLPRO. The ROVGF method[26,27] implemented in Gaussian was also used to obtain the ionization energies using both PBE/6-311G** and MP2/cc-pVDZ geometries.

Two different methods were used to determine the difference between the vertical and adiabatic energies for the lowest ionic states: (a) the vertical ionization energy is simply the difference between the ground state and the ionic state at the neutral equilibrium geometry, while the adiabatic value is given by the difference of the energies (corrected by the zero-point vibrational energy (ZPVE) correction) obtained at both neutral and ionic equilibrium geometries; (b) to use Franck−Condon analysis to obtain the energy difference between the vertical excitation and the position of the 0−0 vibrational band. This analysis was performed in the frame of the Domcke−Cederbaum model,[28] which simply requires the frequencies of the ground state, and the first- and second-order derivatives, with respect to the normal coordinates, of the ion energy, at the geometry of the ground state.

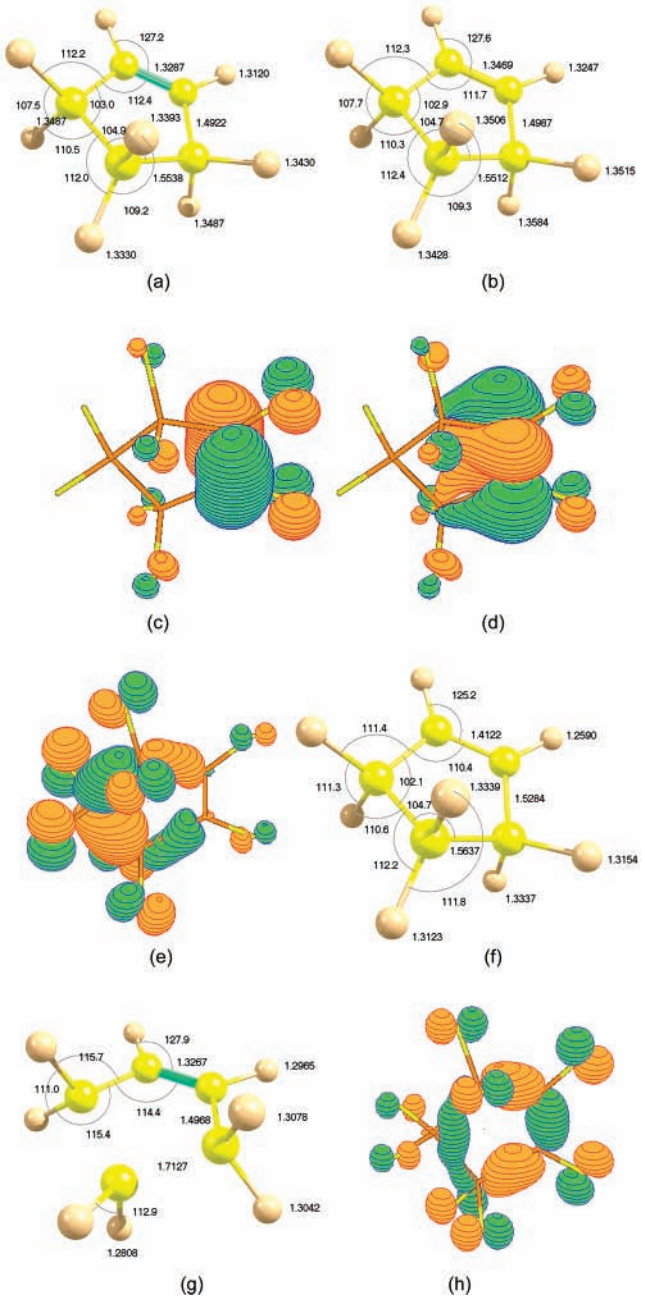

Figure 5. Ground state structure of c-C_5F_8 calculated by (a) the PBE0/6-311G** method, (b) the MP2/cc-pVDZ method, (c) the HOMO (30a′) of c-C_5F_8, (d) the LUMO (22a″) of c-C_5F_8, and (e) the SHOMO (21a″). Ionic states structures (PBE0/6-311G**) of (f) the ^{2}A′ state, (g) the ^{2}A″ state, and (h) HOMO-2, 29a′.

4. Results and Discussion

4.1 Structure and Properties of c-C_5F_8. The calculated geometries in Figure 5a,b show the results from the two calculation methods employed, PBE0/-6311G** and MP2/cc-pVDZ, respectively. To the best of our knowledge, there are no experimental values for the ground state geometry of c-C_5F_8, but our results are very similar to those obtained by Fischer and Cao[29] at the HF, MP2, and B3LYP levels using the 6-31G* basis set.

The calculated electron configuration of the $\tilde{X}^1$A′ ground state of c-C_5F_8 is

(a) core F 1s orbitals $1a''^2\ 1a'^2\ 2a'^2\ 3a'^2\ 2a''^2\ 4a'^2\ 3a''^2\ 5a'^2$

(b) core C 1s orbitals $6a'^2\ 4a''^2\ 7a'^2\ 8a'^2\ 5a''^2$

TABLE 1: Calculated Vertical Excitation Energies (TDDFT/PBE0/6-311++G//PBE0/6-311G**) of the Lowest Lying States of c-C_5F_8 (eV), Oscillator Strengths, and VUV Experimental Data**

symmetry	E (eV)	f_L	HOMO, 30a′ (π)	SHOMO, 21a″ σ(C−C)/n(F)	HOMO-2, 29a″ n(F)	other	exp. (eV)
$\tilde{X}$ ^{1}A′	0.000	ground state					
2 ^{1}A′	7.138	0.0126	$\pi\rightarrow$3s/ σ*(C−F)				7.221
3 ^{1}A′	7.369	0.0020		σ(C−C)/n(F) $\rightarrow\pi$*			
1 ^{1}A″	7.428	0.3064	$\pi\rightarrow\pi$*				7.754
2 ^{1}A″	7.778	0.0047			n(F) $\rightarrow\pi$*		
4 ^{1}A′	8.540	0.0972	$\pi\rightarrow\sigma$*(C−F)				[a]
3 ^{1}A″	8.584	0.0056		σ(C−C)/n(F)$\rightarrow$ 3s/ σ*(C−F)			
4 ^{1}A″	9.072	0.0039		σ(C−C)/n(F) $\rightarrow\sigma$*(C−F)			
5 ^{1}A′	9.120	0.0016			n(F) $\rightarrow$ 3s/ σ*(C−F)		9.523
5 ^{1}A″	9.123	0.0006	$\pi\rightarrow$ 3p				
6 ^{1}A′	9.203	0.0013	$\pi\rightarrow$ 3p				8.837
7 ^{1}A′	9.580	0.0029				n(F) $\rightarrow\pi$*	
6 ^{1}A″	9.626	0.0011				n(F) $\rightarrow\pi$*	
8 ^{1}A′	9.651	0.0004				n(F) $\rightarrow\pi$* + $\pi\rightarrow$ 3d	
9 ^{1}A′	9.728	0.0175				n(F) $\rightarrow\pi$* + $\pi\rightarrow$ 3p + $\pi\rightarrow$ 3d	[a]
10 ^{1}A′	9.747	0.0073				π 3p + $\pi\rightarrow$ 3d + n(F) $\rightarrow\pi$*	9.421
7 ^{1}A″	9.929	<0.0001				n(F) $\rightarrow\pi$*	
11 ^{1}A′	10.023	0.0039			n(F) $\rightarrow\sigma$*(C−F)		
12 ^{1}A′	10.100	0.0186				n(F) $\rightarrow\pi$*	
8 ^{1}A″	10.113	0.0014				n(F) $\rightarrow\pi$*	
9 ^{1}A″	10.223	0.0068		σ(C−C)/n(F) $\rightarrow$ 3p			
10 ^{1}A″	10.279	<0.0001	$\pi\rightarrow$ 3d				
13 ^{1}A′	10.362	0.0042		σ(C−C)/n(F) $\rightarrow$3p			
14 ^{1}A′	10.432	0.0023	$\pi\rightarrow$3d				
11 ^{1}A″	10.521	0.0012				n(F) $\rightarrow\pi$*	
15 ^{1}A′	10.608	0.0059				n(F) $\rightarrow\pi$* +$\pi\rightarrow$ 3d	
16 ^{1}A′	10.624	0.0358				π* 3d + n(F) $\rightarrow\pi$*	[a]
12 ^{1}A″	10.703	0.0039				n(F) $\rightarrow$ 3s/ σ*(C−F)	
17 ^{1}A′	10.721	0.0134				n(F) $\rightarrow$ 3s/ σ*(C−F) + π* $\rightarrow$ 3d	[a]
13 ^{1}A″	10.721	0.0121				n(F) $\rightarrow$ 3s/ σ*(C−F) + n(F) (HOMO^{-2}) $\rightarrow$ 3p	
18 ^{1}A′	10.735	0.0003				n(F) $\rightarrow$ 3s/ σ*(C−F) + $\pi\rightarrow$ 4p	
14 ^{1}A″	10.794	0.0023	$\pi\rightarrow$ 3d				
19 ^{1}A′	10.931	0.0001			n(F) $\rightarrow$ 3p		
15 ^{1}A″	10.957	0.0040	$\pi\rightarrow$ 4s				
16 ^{1}A″	11.001	0.0122		σ(C−C)/n(F) $\rightarrow$ 3p			10.570
20 ^{1}A′	11.012	0.0117				n(F) $\rightarrow\pi$*	
17 ^{1}A″	11.040	0.0001				n(F) $\rightarrow\pi$* + n(F) $\rightarrow$ 3s/ σ*(C−F)	
18 ^{1}A″	11.081	0.0182			n(F) $\rightarrow$ 3p		
21 ^{1}A′	11.088	0.0022	$\pi\rightarrow$ 4p				
19 ^{1}A″	11.131	0.0057		σ(C−C)/n(F) $\rightarrow$ 3d			
22 ^{1}A′	11.161	0.0156				n(F) $\rightarrow$ 3s/ σ*(C−F) + n(F) $\rightarrow\pi$*	10.401

[a] See discussion in text.

(c) σ(CF) orbitals 9a′^{2} 6a″^{2} 10a′^{2} 11a′^{2} 7a″^{2} 12a′^{2} 8a″^{2} 13a′^{2}

(d) σ(CC) orbitals 14a′^{2} 15a′^{2} 9a″^{2} 16a′^{2} 10a″^{2}

(e) n(F) lone pairs 17a′^{2} 18a′^{2} 11a″^{2} 19a′^{2} 12a″^{2} 20a′^{2} 13a″^{2} 21a′^{2} 22a′^{2} 14a″^{2} 15a″^{2} 23a′^{2} 24a′^{2} 16a″^{2} 17a″^{2} 25a′^{2} 26a′^{2} 18a″^{2} 27a′^{2} 19a″^{2} 20a″^{2} 28a′^{2} 29a′^{2} 21a″^{2}

(f) π(C=C)/n(F) lone pair 30a′^{2}.

The highest occupied molecular orbital (HOMO) in the neutral ground state, 30a′, represented in Figure 5c with the MOLDEN software,[30] is calculated to be mainly π(C=C) and only partial F lone pair character. The lowest unoccupied molecular orbital (LUMO) is essentially the π*(C=C) (22a″) orbital (Figure 5d) with a slight bonding π character with the adjacent carbon atoms, as in butadiene. The second highest occupied MO (SHOMO) has an important σ(C−C) bonding character mixed with F lone pair contribution (Figure 5e). This is also the case for several lower lying MO's, so that the distinction between σ(C−C) and n(F) may be somewhat arbitrary.

In its ground neutral electronic state, c-C_5F_8 has C_s symmetry with 33 modes of vibration. In the present high resolution absorption spectrum, for some excited electronic states, resonant vibrational modes with mean excitation energies of 0.219 and 0.148 eV were observed (see Figure 1). In the absence of any experimental data on the excitation energies for the vibrational modes of c-C_5F_8 in the literature, we have labeled these features ν_A′ and ν_B′, respectively, and identified them on the basis of our PES (see section 4.5) as being mainly due to contributions of the C=C stretching and C−C stretching modes. The calculated transition energies, oscillator strengths and the main character of the wave function are shown in Tables 1 (TDDFT results) and 2 (EOM-CCSD results). Most calculated transitions have very low intensities, because of their Rydberg character. There are rather large differences between the two sets of results. It is well-known[16,20] that TDDFT methods do not accurately describe Rydberg states. These differences are more surprising for valence states since, as detailed in a recent review,[31] the EOM-CCSD method is very accurate for the description of electronic spectra of small molecules. However, in the case of c-C_5F_8, it is possible that the limitation to di-excitations in the CCSD model is insufficient, due to the large number of electrons. It should be noted that a recent study on fluoroethylenes,[32] using the SAC-CI method, also found discrepancies of several tenths of an electron volt, even for the $\pi-\pi$* transition.

TABLE 2: Calculated Vertical Excitation Energies (EOM-CCSD/cc-pVDZ + R//MP2/cc-pVDZ) of the Lowest Lying States of c-C_5F_8 (eV), Oscillator Strengths, and VUV Experimental Data

symmetry	E (eV)	f_L	$\langle r2 \rangle$	HOMO, 30a′ (π)	SHOMO, 21a″ σ (C−C)/n(F)	HOMO^{-2}, 29a″ n(F)	exp. (eV)
$\tilde{X}$ ^{1}A′	0.000	ground state	158				
2 ^{1}A′	7.569	0.0183	175	$\pi \rightarrow$ 3s/π*(C−F)			7.221
1 ^{1}A″	8.119	0.3503	158	$\pi \rightarrow \pi$*			7.754
2 ^{1}A″	8.615	0.0066	156			n(F) $\rightarrow \pi$*	[a]
3 ^{1}A′	8.664	0.0019	158		σ (C−C)/n(F) $\rightarrow \pi$*		
4 ^{1}A′	9.374	0.0152	227	$\pi \rightarrow$ 3p			8.837
3 ^{1}A″	9.441	<0.0001	237	$\pi \rightarrow$ 3p			
4 ^{1}A″	9.533	0.0029	183		σ (C−C)/n(F) $\rightarrow$ 3s/ σ *(C−F)		9.523
5 ^{1}A′	9.536	0.0010	248	$\pi \rightarrow \sigma$ *(C−F)			
6 ^{1}A′	9.705	0.0024	252	$\pi \rightarrow$ 3p			
7 ^{1}A′	9.840	0.0004	179			n(F) $\rightarrow$ 3s/ σ *(C−F)	
8 ^{1}A′	9.933	0.0857	203	$\pi \rightarrow \sigma$ *(C−F)			10.570
5 ^{1}A″	10.005	0.0029	167		σ (C−C)/n(F) $\rightarrow \sigma$ *(C−F)		
9 ^{1}A′	10.133	0.0070	304	$\pi \rightarrow$ 3d			9.421
6 ^{1}A″	10.271	<0.0001	323	$\pi \rightarrow$ 3d			
7 ^{1}A″	10.283	0.0004	334	$\pi \rightarrow$ 3d			
10 ^{1}A′	10.309	<0.0001	338	$\pi \rightarrow$ 3d			
11 ^{1}A′	10.398	0.0071	338	$\pi \rightarrow$ 3d			
8 ^{1}A″	10.465	<0.0001	462	$\pi \rightarrow$ 4p			
12 ^{1}A′	10.470	0.0006	482	$\pi \rightarrow$ 4s			
13 ^{1}A′	10.548	0.0076	497	$\pi \rightarrow$ 4p			
14 ^{1}A′	10.595	0.0010	544	$\pi \rightarrow$ 4p			
9 ^{1}A″	10.698	0.0004	235		σ (C−C)/n(F) $\rightarrow$ 3p		
10 ^{1}A″	10.849	<0.0001	658	$\pi \rightarrow$ 4d			
11 ^{1}A″	10.887	<0.0001	607	$\pi \rightarrow$ 4d			
12 ^{1}A″	10.942	0.0024	307		σ (C−C)/n(F) $\rightarrow$ 3p		10.570

[a] See discussion in text.

TABLE 3: Vibrational Assignments in the 8.5−11.0 eV Absorption Band of c-C_5F_8[a]

energy[b]	assignment	$\Delta E1$ (ν_A′)	ΔE (ν_B′)	energy[b]	assignment	ΔE (ν_A′)	ΔE (ν_B′)
8.837	ν_{00}			9.191 [s]	ν_{00}		
9.056 [d]	ν_A′	0.219		9.350 [w]	ν_B′		0.159
9.204	ν_A′ + ν_B′		0.148	9.407 [s]	ν_A′	0.216	
9.287	2ν_A′	0.231		9.552 [s]	ν_B′ + ν_A′		
9.421	ν_A′ + 2ν_B′	0.217		9.619 [s]	2ν_A′	0.212	
9.493 [s]	3ν_A′	0.206		9.778	ν_B′ + 2ν_A′	0.205	
9.656	νA′ + 3ν_B′	0.235		9.824 [s]	3ν_A′	0.205	
9.686 [s]	4ν_A′	0.193		9.983 [s]	ν_B′ + 3ν_A′	0.205	
9.864	ν_A′ + 4ν_B′	0.208		10.031	4ν_A′	0.207	
9.895	5ν_A′	0.209		10.188 [s]	ν_B′ + 4ν_A′	0.205	
10.064	ν_A′ + 5ν_B′	0.200		10.238	5ν_A′	0.207	
10.113 [w]	6ν_A′	0.218		10.410	ν_B′ + 5ν_A′	0.222	
10.272	ν_A′ + 6ν_B′	0.208		10.436 [w]	6ν_A′	0.198	
10.315 [d]	7ν_A′	0.202		10.606	ν_B′ + 6ν_A′	0.196	
10.481	ν_A′ + 7ν_B′	0.209		10.643 [d]	7ν_A′	0.207	
10.525 [d]	8ν_A′	0.210					
10.670 [w]	ν1′ + 8ν_B′	0.189					
10.744 [w]	9ν_A′	0.219					

[a] This work (energies are in eV). [b] [d] = diffuse structure; [s] = shoulder; [w] = weak feature.

4.2. Neutral Excited States. The high-resolution absolute VUV photoabsorption spectrum of c-C_5F_8 was recorded between 6.0 and 11.0 eV using the Aarhus Synchrotron Facility and is shown in Figure 1. Four absorption bands centered at 7.221, 7.754, 8.837, and 9.523 eV, respectively, are observed. All bands are quite broad (Figure 1), suggesting rapid dissociation into neutral radicals, with fine structure being observed in the latter (Figure 2 and Table 3) and reported here for the first time. According to the present calculations (Tables 1 and 2), the first band is due to a Rydberg/valence $\pi \rightarrow$ 3s/σ*(C−F) A′ transition. It is noteworthy that the TDDFT value (7.221 eV) is in better agreement with experiment than the EOM-CCSD result (7.569 eV). The second band, which is the most intense, corresponds to the $\pi \rightarrow \pi$* A″ transition. When compared to the measured value of 7.754 eV, the TDDFT result is slightly underestimated (7.428 eV), while the EOM-CCSD value is too high (8.119 eV).

The situation is much less clear for the third band at 8.837 eV, since there are large discrepancies between the two sets of calculations: while TDDFT predicts an intense ($f = 0.0972$) $\pi \rightarrow \sigma$*(C−F) A′ transition to occur at 8.540 eV, the EOM-CCSD counterpart is calculated at much higher energy (9.993 eV). According to EOM-CCSD, the only possible candidate could be the $\pi \rightarrow$ 3p transition calculated at 9.372 eV, but its intensity is rather low (0.0152). Both methods also predict numerous transitions in this energy range, arising mainly from the HOMO and the SHOMO, but their intensities are very weak as a result of their Rydberg nature. The fact that the SHOMO σ(C−C)/n(F) $\rightarrow \pi$* transition is weak may be rationalized by the fact that these MO's have densities on opposite parts of the molecule (Figure 5).

The background level is relatively high in the 8.5−10 eV energy region; therefore there might be a contribution from an

TABLE 4: Calculated Vibrational Energies for Both Neutral Ground and Lowest Ionic States of c-C_5F_8 (Energies Are in cm^{-1})

C_S modes	calculation: neutral ground state[a]	experiment[b]	calculation: ionic $^2A'$ state[a]	calculation: ionic $^2A''$ state[a]
a′	1841	1770	1711	1856
	1417	1386	1402	1420
	1361	1327	1363	1415
	1248	1219	1268	1315
	1207	1180	1259	1283
	1172	1144	1195	1171
	1031	1008	1032	929
	682	663	687	691
	639	617	637	656
	623	603	579	590
	512	499	470	465
	437	430	411	422
	351	347	359	328
	312	312	299	272
	248	252	248	247
	219	234	187	200
	175	187	150	173
	41	-	59	52
a″	1428	1389	1539	1431
	1323	1300	1346	1305
	1181	1211	1222	1282
	1136	1106	1086	1045
	1007	985	1018	828
	874	889	859	738
	715	721	739	648
	608	627	608	473
	451	444	438	417
	418	419	376	376
	313	312	286	284
	271	274	260	275
	258	252	225	211
	245	234	195	127
	99	100	75	i129

[a] This work (PBE0/6-311G**). [b] See reference 35.

underlying σ^* dissociative state in this region. Indeed, the calculations predict a σ^* state at 9.536, as shown in Table 2. This state is therefore very likely dissociative.

4.3. Vibrational Excitation in the Energy Range 8.5−11.0 eV. The VUV spectrum in this energy region (Figure 2) is characterized by a fine structure pattern coupled with the Rydberg series (see next section). Two transitions have been assigned to 8.837 (8.115 Mb) and 9.191 eV (6.733 Mb) in Table 3. These proposed progressions have been identified by calculations, using the Domcke−Cederbaum[28] procedure described above, as being the C═C stretching and C−C stretching modes, with mean energies of 0.219 and 0.148 eV, and labeled as (ν_A') and (ν_B'), respectively. Mode A′ is the 1770 cm^{-1} (0.232 eV) (C═C stretch nature as confirmed by theory) reported in Table 4, while mode B′ could be the 1185 (0.148 eV) and/or 1144 cm^{-1} (0.142 eV) modes (C−C stretch).

4.4. Rydberg Series. The cross section above 7 eV shows contributions from several assigned Rydberg structures (Figures 1 and 2), members of series converging to the three lowest ionization limits at 11.288, 12.944, and 13.791 eV, respectively (Figure 4), and mainly due to the promotion of a fluorine lone pair electron.

The peak positions, E_n, must fit the Rydberg formula: $E_n = E_i - R/(n - \delta)^2$, where E_i is the ionization energy, n is the principal quantum number of the Rydberg orbital of energy E_n, R is the Rydberg constant, and δ is the quantum defect resulting from the penetration of the Rydberg orbital into the core.

TABLE 5: Energy Values, Quantum Defect, and Assignment of the Rydberg Series Converging to the Ionic Electronic Ground State, $(30a')^{-1}$ (Energies Are in eV)

energy	quantum defect	assignment	ΔE (ν_A')
7.221	1.17	3s	
9.747[a]	1.03	4s	
10.410[b]	1.06	5s	
10.744	1.00	6s	
8.837	0.64	3p	
10.080	0.64	4p	
10.550	0.70	5p	
10.820	0.61	6p	
11.040		$6p + 1\nu_A'$	0.220
11.230		$6p + 2\nu_A'$	0.190
11.390[a]		$6p + 3\nu_A'$	0.160
11.610		$6p + 4\nu_A'$	0.220
11.820		$6p + 5\nu_A'$	0.210
9.421	0.30	3d	
10.289	0.31	4d	
10.670	0.31	5d	

[a] Peak shoulder. [b] Broad feature.

Vibrational excitation associated with some Rydberg states are presented in detail in Tables 5, 6, and 7. However, in order to avoid congestion in the Rydberg series, we have not labeled them in the figures. The two modes being excited are those already reported for the valence excitation in the 8.5−10.0 eV energy region.

4.4.1. Rydberg Series Converging to the Lowest Electronic Ionic Ground State 30 a'^{-1}. The origin of three Rydberg series at 7.221, 8.837, and 9.421 eV have been identified to correspond to the 3s, 3p, and 3d transitions, with quantum defects δ of 1.17, 0.64, and 0.30, respectively (Table 5). The 3s member has a slightly high quantum defect for an s series, but that seems reasonable because of the mixing valence/Rydberg character. A comparison of the calculated vertical excitation energies in Tables 1 and 2 with the present VUV photoabsorption and EELS features (Figures 1 and 3) show some tentative assignments for the observed structure.

4.4.2. Rydberg Series Converging to the First Electronic Excited Ionic State 21 a''^{-1}. The first member of the lowest energy series (Table 6, Figure 2) observed converging to the first ionic electronic excited-state has been assigned to the fluorine lone pair electrons (n(F) → 3s) lying at 9.523 eV with a quantum defect of $\delta = 1.00$. There are three other series: np, np′, and nd, with their first terms being assigned to $n = 3$ at 10.570, 10.744, and 11.330 eV, with quantum defects $\delta = 0.61$, 0.51 and 0.10, respectively. The $n = 5$ at 12.270 eV and $n = 3$ at 11.330 eV are broad features and may also contain contributions from 4s and 3p′, respectively, both converging to the second electronic ionic excited state.

4.4.3. Rydberg Series Converging to the Second Excited Ionic State 29a'^{-1}. The first term of five series has been assigned to converge to the ionic energy 13.791 eV (Table 7, Figures 1 and 2). The energy position of the ns, np, np′, np″, and nd, lying at 10.401, 11.330, 11.450, 11.770, and 12.220 eV corresponds to quantum defects $\delta = 0.99$, 0.65, 0.59, 0.41 and 0.09, respectively. There are several features at 13.070, 13.210, and 13.390 eV that could also be members of different series converging to higher energy levels that can be explained by the broadness of the peaks observed, as shown in the EEL spectrum in the 13−14 eV region.

4.5. Ionic States. Figure 4 shows the bands associated with the ionic states of c-C_5F_8. The energy positions of the observed features are summarized in Table 8. The shape of the lowest

TABLE 6: Energy Values, Quantum Defect, and Assignment of the Rydberg Series Converging to the Ionic Electronic First Excited State, $(21a'')^{-1}$ (Energies Are in eV)

energy	quantum defect	assignment	ΔE (ν_A')	energy	quantum defect	assignment	ΔE (ν_A')
9.523[a]	1.00	3s		12.270[b]	0.51	5p′	
11.430[a]	1.00	4s		12.490	0.53	6p′	
11.610		4s + 1ν_A'	0.180				
12.110[a]	0.96	5s		12.840	0.56	12p′	
				13.030		12p′ + 1ν_A'	0.190
10.570[a]	0.61	3p					
11.700	0.69	4p		11.330	0.10	3d	
12.230[a]	0.64	5p		11.530		3d′ + 1ν_A'	0.200
12.400		5p + 1ν_A'	0.170	11.700		3d′ + 2ν_A'	0.170
12.580		5p + 2ν_A'		11.860		3d′ + 3ν_A'	0.160
				12.020		3d′ + 4ν_A'	0.160
12.750	0.62	9p		12.190		3d′ + 5ν_A'	0.170
				12.350		3d′ + 6ν_A'	0.160
10.744	0.51	3p′		12.540		3d′ + 7ν_A'	0.190
11.820	0.52	4p′		12.070	0.06	4d	
11.990		4p′ + 1ν_A'	0.170	12.400	0.00	5d	
12.160		4p′ + 2ν_A'	0.170				
12.320		4p′ + 3ν_A'	0.160	12.660	0.08	7d	

[a] Peak shoulder. [b] Broad feature.

TABLE 7: Energy Values, Quantum Defect, and Assignment of the Rydberg Series Converging to the Ionic Electronic Second Excited State, $(29a')^{-1}$ (Energies Are in eV)

energy	quantum defect	assignment	ΔE (ν_A')	energy	quantum defect	assignment	ΔE (ν_A')
10.401	0.99	3s		12.720[a]	0.44	4p″	
12.270	1.00	4s		13.140	0.43	5p″	
12.930	1.03	5s		13.340 (sh)	0.51	6p″	
13.210	1.16	6s					
13.390	1.17	7s		13.560	0.33	8p″	
11.330	0.65	3p		12.220 (sh)	0.06	3d	
12.580	0.65	4p					
13.070	0.66	5p		13.210	0.16	5d	
13.310	0.68	6p		13.390	0.17	6d	
13.490		6p + 1ν_A'	0.180	13.560		6d + 1ν_A'	0.170
				13.720		6d + 2ν_A'	0.160
11.450	0.59	3p′		13.870		6d + 2ν_A' + 1ν_B'	
12.620 (sh)	0.59	4p′		13.920		6d + 3ν_A'	0.200
13.070	0.65	5p′					
13.340 (s)	0.51	6p′		13.620	0.08	9d	
13.460 (s)	0.59	7p′		13.790		9d + 1ν_A'	0.170
				13.980		9d + 2ν_A'	0.190
11.770	0.41	3p″		13.650	0.18	10d	
11.940		3p″ + 1ν_B'	0.170				

[a] Peak shoulder

energy ionic band (Figure 4b) is quite broad, and superimposed on it there is a fine structure, whose maximum intensity lies at 11.696 ± 0.002 eV, corresponding to the vertical ionization energy. This value is compared to the calculations in Table 8. Despite their computational cost, the RCCSD and RCCSD(T) results are too low by ~1 eV. The UPBE0 method is better (11.374 eV), but the best results are obtained with the ROVGF method, especially with the cc-pVDZ basis set (11.776 eV).

Photoelectron spectroscopy can give both the adiabatic (or at least the most probable value of it) and the vertical ionization energies, the values of which tend to differ significantly whenever there is a large change in equilibrium molecular geometry on ionization.[14] In order to obtain the theoretical adiabatic ionization energy, the geometry of the $30a'^{-1}$ state was optimized at the UPBE0/6-311G** level, as shown in Figure 5f. As shown in the third column of Table 4, the calculated frequencies prove that this geometry corresponds to a true minimum. The main difference with the neutral geometry is a larger C═C bond due to the weakening of the π MO (+0.1 Å). After zero-point energy (ZPE) correction, the calculated adiabatic energy is predicted to be 10.832 eV, which is too low, but the theoretical difference between vertical and adiabatic energies (0.541 eV) is close to the observed one (0.488 eV). Interestingly, the same quantity is calculated to be 0.54 eV using the Domcke−Cederbaum vibrational analysis.

The vibrational pattern found in this band (Table 9) has been assigned to the excitation of the C═C stretching (ν_A') and to a contribution of the C−C stretching (ν_B') modes, with mean energies of 0.200 and 0.140 eV, respectively. The threshold for c-$C_5F_8^+$ has been quoted to be (11.6 ± 0.7) eV,[6] in good agreement with the maximum position of the present first ionic band. The shape of this first ionic band suggests that the parent ion must have a short lifetime.

The absence of vibrational structure in the second electronic band of the PES centered at 12.944 eV (which is very close to the calculated ROVGF/cc-pVDZ value of 13.047 eV) could be due to a very fast decomposition of the c-$C_5F_8^+$ molecular ion, although the ionization measurements of Jiao et al.[6] do not report

TABLE 8: Calculated and Experimental He(I) Photoelectron Ionization Energies of c-C_5F_8 (Energies Are in eV)

configuration	(U)PBE0[a]	ROVGF[a]	ROVGF[b]	RCCSD[b]	RCCSD(T)[b]	exp.[c]
30 a′ $^{-1}$	11.374	11.938	11.776	10.594	10.534	11.696
21 a″ $^{-1}$	12.354	13.177	13.047	12.178	11.826	12.944
29 a′ $^{-1}$		13.968	13.812			13.791
28 a′ $^{-1}$		15.686	15.872			15.59
20 a″ $^{-1}$		15.707	15.538			15.59
19 a″ $^{-1}$		15.847	15.482			15.59
27 a′ $^{-1}$		15.962	15.573			15.59
18 a″ $^{-1}$		16.142	16.001			15.98
26 a′ $^{-1}$		16.178	15.910			15.98
25 a′ $^{-1}$		16.641	16.407			16.67
17 a″ $^{-1}$		16.916	16.703			16.67
16 a″ $^{-1}$		17.151	16.882			16.67
24 a′ $^{-1}$		17.345	17.094			17.37
15 a″ $^{-1}$		17.428	17.192			17.37
23 a′ $^{-1}$		17.432	17.229			17.37
14 a″ $^{-1}$		17.721	17.463			17.37
22 a′ $^{-1}$		18.399	18.113			18.38
21 a′ $^{-1}$		19.541	19.287			19.51
13 a″ $^{-1}$		19.765	19.533			19.51
12 a″ $^{-1}$		19.940	19.679			19.51
20 a′ $^{-1}$		19.978	19.718			19.51

[a] This work. Values obtained at the PBE0/-6311G** geometry. [b] This work. Values obtained at the MP2/cc-pVDZ geometry. [c] This work.

TABLE 9: Energy Positions and Vibrational Analysis of Features Observed in the Photoelectron Bands of c-C_5F_8[a]

energy (eV)[b]	analysis	ΔE (ν_A') (eV)	ΔE (ν_B') (eV)
11.288	ν_{00}, adiabatic IE_1		
11.431 (?)	$\nu_{B'}$		0.143
11.499	$1\nu_{A'}$	0.211	
11.631 (?)	$1\nu_{A'} + \nu_{B'}$		0.132
11.696	$2\nu_{A'}$, vertical IE_1	0.197	
11.822 (?)	$2\nu_{A'} + \nu_{B'}$		0.126
11.892	$3\nu_{A'}$	0.196	
12.037 (?)	$3\nu_{A'} + \nu_{B'}$		0.145
12.107	$4\nu_{A'}$	0.215	
12.944	vertical IE_2		
13.482	ν_{00}, adiabatic IE_3		
13.636	$\nu_{B'}$		0.154
13.685	$\nu_{A'}$	0.203	
13.791	$1\nu_{A'} + \nu_{A'}$		0.155
13.857 (?)	$2\nu_{A'}$	0.172	
13.972 (?)	$2\nu_{A'} + \nu_{B'}$		0.181
15.59	vertical IE_4		
15.98	vertical IE_5		
16.67	vertical IE_6		
17.37	vertical IE_7		
18.38	vertical IE_8		
19.51	vertical IE_9		

[a] Uncertainties of the values given are ±0.002 eV for IE_1-IE_3 and ±0.02 eV for IE_4-IE_9. [b] (?) means uncertainty to peak/structure position.

any fragmentation yield in this energy region. In order to test this hypothesis, the geometry of the 21a″$^{-1}$, i.e., the SHOMO^{-1}, ionic state was optimized at the UPBE0/6-311G** level (Figure 5g). This state appears to be stable, with a lengthening of the C−C bonds consistent with the shape of the SHOMO (Figure 5e). However, the calculated vibrational modes (last column of Table 4) indicate that this structure is a saddle point with an a″ imaginary frequency, corresponding to the deformation of the carbon ring. Removing the C_s constraint during the optimization leads to the ^{2}A′ (HOMO^{-1}) ionic state, so it is impossible to obtain the geometry of the ^{2}A″ state. Nonetheless, the calculations prove without ambiguity that this state is stable, and the absence of apparent vibrational fine structure could be due to numerous overlapping vibration peaks.

The third ionic band centered at 13.791 eV (Figure 4c) also shows some evidence of excitation of the two vibrational (ν_A') and (ν_B') modes (Table 9). This value is in excellent agreement with the ROVGF/cc-pVDZ calculated value at 13.812 eV. The calculations also show that this band has to be assigned to the (29a′)$^{-1}$, i.e., the HOMO-2 state. The appearance threshold of the fragment ion $C_4F_6^+$ has been reported at (14.2 ± 0.7) eV,[6] which can be closely related to the nature of this ionic band. In fact, the background level is relatively high, suggesting a transition into a repulsive energy surface of the molecular ion leading to dissociation. The calculations are not able to test this hypothesis, but the delocalized character of the 29a′ MO (Figure 5h) does not seem to indicate a fragmentation into $C_4F_6^+ + CF_2$.

The other bands' positions, at higher energies, are listed in Table 9. According to the ROVGF calculations, their high intensity and absence of vibrational structure might be explained by the overlap of ionization bands of the quasi-degenerate lower lying (mainly lone pairs) MO's of the molecule.

The present PES also shows a few extra sharp features between 13.2 and 14.2 eV bands that are due to the Ar^+ calibration $^2P_{3/2}$ He(I)γ line and the $^2P_{3/2}$, $^2P_{1/2}$ He(I)β line, respectively. These features have been shown not to interfere with the observed patterns.

4.6. Photolysis Rates and Local Lifetimes. The absolute cross section values of c-C_5F_8 can be used to model its atmospheric destruction by UV photolysis as a function of altitude. Details of the program are presented in a previous publication by Limão-Vieira et al.[33] Photolysis rates at a given wavelength were calculated as the product of the solar actinic flux,[34] and the molecular photoabsorption cross section at 1 km altitude steps from the surface up to the stratopause (50 km). At each altitude, a total photolysis rate may then be calculated by summing over the individual photolysis rates for that altitude. The reciprocal of the total photolysis rate for a given altitude gives the local photolysis lifetime at that altitude, i.e., the time taken for the molecule to photodissociate at the altitude, assuming that the solar flux remains constant. The local lifetimes and the photolysis rates are shown in Figure 6, where, for the former, we assume that the quantum yield for dissociation is

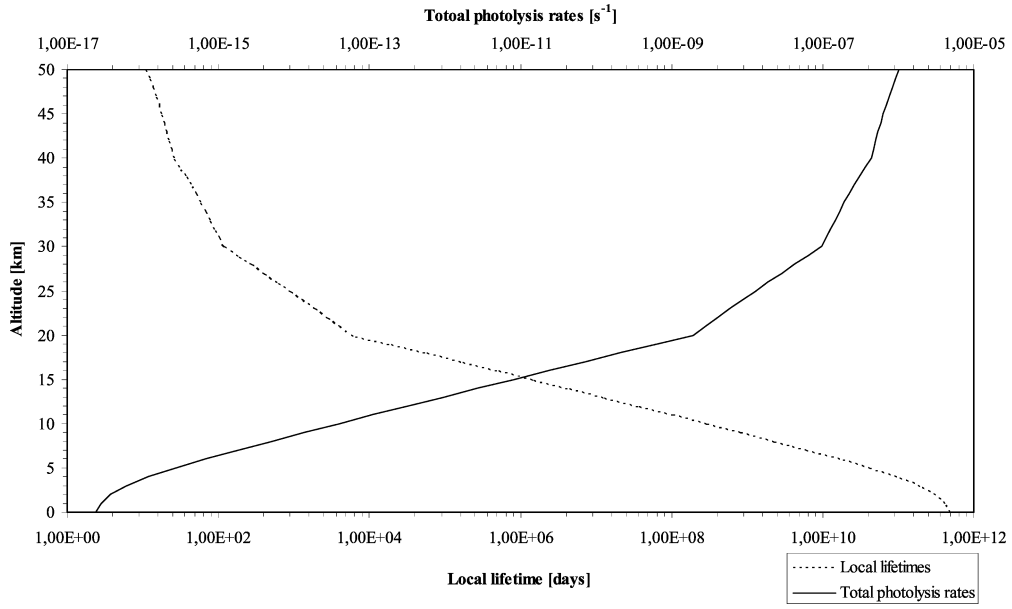

Figure 6. The local lifetime of c-C_5F_8 between 0 and 50 km obtained from its photoabsorption spectrum (Figure 1).

unity. The results show that the local photolysis lifetime of c-C_5F_8 varies from about 17 years at 20 km to a few days at 40−50 km. Therefore, it indicates that c-C_5F_8 will be stable to photolysis in the troposphere but can be broken up reasonably at higher altitudes. We have recently reported high-resolution Fourier transform infrared (FTIR) spectra[35] showing a strong infrared absorption cross section in the wavelength region of the earth's atmospheric window (800−1300 cm^{-1}), such that a long tropospheric lifetime may lead to a GWP of around 60 times that of CO_2 in a 100 years time horizon.

5. Conclusions

The present results are the first comprehensive set of experimental data on the spectroscopy of octafluorocyclopentene (c-C_5F_8) in the 6−14 eV energy region. An electron energy loss spectrum (EELS) was also recorded in the electric dipolar interaction (100 eV incident energy, ∼0° scattering angle) over the 5−14 eV energy loss range. In both spectra a fine structure is observed in the 10 eV energy region that has been assigned to specific vibrational modes. The VUV spectrum shows four absorption bands, centered at 7.221, 7.754, 8.837, and 9.191 eV with cross-sectional values of 11.440, 21.084, 8.116, and 6.733 Mb, respectively.

Ab initio calculations on the vertical excitation energies and oscillator strengths were used in the assignment of the spectral transitions. When compared to experiment the EOM-CCSD method tends to overestimate the excitation energy, while TDDFT values seem to be in better agreement. For ionic states, the ROVGF energies are in very good agreement with experiment, while CC values are too low by about 1 eV.

The measured photoabsorption cross sections have been used to derive the local lifetime in the Earth's atmosphere (0−50 km), showing that octafluorocyclopentene may have a short residence time in the upper atmosphere but a longer residential time in the lower stratosphere, leading to a significant GWP.

References and Notes

(1) Vasekova, E.; Drage, E. A.; Smith, K. M.; Mason, N. J. *J. Quant. Spectrosc. Radiat. Transfer* **2006**, *102*, 418−424.
(2) (a) Motomura, H.; Imai, S.-I.; Tachibana, K. *Thin Solid Films* **2000**, *374*, 243−248; (b) Takahashi, K.; Itoh, A.; Nakamura, T.; Tachibana, K. *Thin Solid Films* **2000**, *374*, 303−310.
(3) Mason, N. J.; Dawes, A.; Mukerji, R.; Drage, E. A.; Vasekova, E.; Webb, S. M.; Limão-Vieira, P. *J. Phys. B* **2005**, *38*, S893−S911.
(4) Limão-Vieira, P.; Vasekova, E.; Giuliani, A.; Lourenço, J. M. C.; Santos, P. M.; Duflot, D.; Hoffmann, S. V.; Mason, N. J.; Delwiche, J.; Hubin-Franskin, M.-J. *Phys. Rev. A* **2007**, *76*, 032509-1−032509-10.
(5) Chutjian, A.; Alajajian, S. H *J. Phys. B* **1985**, *18*, 4159−4167.
(6) Jiao, C. Q.; DeJoseph, C. A., Jr.; Garscadden, A. *J. Phys. D* **2005**, *38*, 1076−1080.
(7) Parkes, M. A.; Ali, S.; Tuckett, R. P.; Mickhailov, V. A.; Mayhew, C. A. *Phys. Chem. Chem. Phys.* **2007**, *9*, 5222−5231.
(8) Nakamura, T.; Motomura, H.; Tachibana, K. *Jpn. J. Appl. Phys.* **2001**, *40*, 847−854.
(9) Nakamura, T.; Tachibana, K. *Appl. Phys. Lett*. **2002**, *80*, 3904−3906.
(10) Eden, S.; Limão-Vieira, P.; Hoffmann, S. V.; Mason, N. J. *Chem. Phys.* **2006**, *323*, 313−333.
(11) Motte-Tollet, F.; Hubin-Franskin, M.-J.; Collin, J. E. *J. Chem. Phys.* **1992**, *97*, 7314−7322.
(12) Giuliani, A.; Delwiche, J.; Hoffmann, S. V.; Limão-Vieira, P.; Mason, N. J.; Hubin-Franskin, M.-J. *J. Chem. Phys.* **2003**, *119*, 3670−3680.
(13) Delwiche, J.; Natalis, P.; Momigny, J.; Collin, J. E. *J. Electron Spectrosc. Relat. Phenom.* **1973**, *1*, 219−225.
(14) Eland, J. H. D. *Photoelectron Spectroscopy*; Butterworth & Co., Ltd.: London, 1984; p 60.
(15) Minnhagen, L. *J. Opt. Soc. Am*. **1973**, *63*, 1185−1198.
(16) Dreuw, A.; Head-Gordon, M. *Chem. Rev*. **2005**, *105*, 4009−4037.
(17) Aquilante, F.; Barone, V.; Roos, B. O. *J. Chem. Phys*. **2003**, *119*, 12323−12334.
(18) Adamo, C.; Barone, V. *J. Chem. Phys*. **1999**, *110*, 6158−6170.
(19) Frisch, M. J.; Trucks, G. W.; Schlegel, H. B.; Scuseria, G. E.; Robb, M. A.; Cheeseman, J. R.; Montgomery, J. A., Jr.; Vreven, T.; Kudin, K. N.; Burant, J. C.; Millam, J. M.; Iyengar, S. S.; Tomasi, J.; Barone, V.; Mennucci, B.; Cossi, M.; Scalmani, G.; Rega, N.; Petersson, G. A.; Nakatsuji, H.; Hada, M.; Ehara, M.; Toyota, K.; Fukuda, R.; Hasegawa, J.; Ishida, M.; Nakajima, T.; Honda, Y.; Kitao, O.; Nakai, H.; Klene, M.; Li, X.; Knox, J. E.; Hratchian, H. P.; Cross, J. B.; Bakken, V.; Adamo, C.; Jaramillo, J.; Gomperts, R.; Stratmann, R. E.; Yazyev, O.; Austin, A. J.; Cammi, R.; Pomelli, C.; Ochterski, J. W.; Ayala, P. Y.; Morokuma, K.; Voth, G. A.; Salvador, P.; Dannenberg, J. J.; Zakrzewski, V. G.; Dapprich, S.; Daniels, A. D.; Strain, M. C.; Farkas, O.; Malick, K. D. Rabuck, A. D.; Raghavachari, K.; Foresman, J. B.; Ortiz, J. V.; Cui, Q.; Baboul, A. G.; Clifford, S.; Cioslowski, J.; Stefanov, B. B.; Liu, G.; Liashenko, A.; Piskorz, P.; Komaromi, I.; Martin, R. L.; Fox, D. J.; Keith, T.; Al-Laham, M. A.; Peng, C. Y.; Nanayakkara, A.; Challacombe, M.; Gill, P. M. W.; Johnson,

B.; Chen, W.; Wong, M. W.; Gonzalez, C.; Pople, J. A. *Gaussian 03*, revision D.01; Gaussian, Inc.: Wallingford, CT, 2004.

(20) Serrano-Andres, L.; Merchan, M. *J. Mol. Struct. (THEOCHEM)* **2005**, *729*, 99−108.

(21) Hampel, C.; Peterson, K.; Werner, H.-J. *Chem. Phys. Lett*. **1992**, *190*, 1−12.

(22) Werner H.-J.; Knowles, P. J.; Lindh, R.; Manby, F. R.; Schütz, M.; Celani, P.; Korona, T.; Rauhut, G.; Amos, R. D.; Bernhardsson, A.; Berning, A.; Cooper, D. L.; Deegan, M. J. O.; Dobbyn, A. J.; Eckert, F.; Hampel, C.; Hetzer, G.; Lloyd, A. W.; McNicholas, S. J.; Meyer, W.; Mura, M. E.; Nicklass, A.; Palmieri, P.; Pitzer, R.; Schumann, U.; Stoll, H.; Stone, A. J.; Tarroni, R.; Thorsteinsson, T. *MOLPRO*: *A Package of Ab Initio Programmes*, version 2006.1; University College Cardiff Consultants, Ltd.: Cardiff, U.K., 2006 (http://www.molpro.net).

(23) Kaufmann, K.; Baumeister, W.; Jungen, M. *J. Phys. B* **1989**, *22*, 2223−2240.

(24) Knowles, P. J.; Hampel, C. Werner, H.-J. *J. Chem. Phys*. **1993**, *99*, 5219−5227.

(25) Watts, J. D.; Gauss, J.; Bartlett, R. J. *J. Chem. Phys*. **1993**, *98*, 8718−8733.

(26) Ortiz, J. V.; Zakrzewski, V. G.; Dolgounircheva, O. In *Conceptual Perspectives in Quantum Chemistry*; Calais, J.-L., Kryachko, E., Eds.; Kluwer Academic: Norwell, MA, 1997; pp 465−518.

(27) Ortiz, J. V. *J. Chem. Phys*. **1988**, *89*, 6348−6352.

(28) Köppel, H.; Domcke, W.; Cederbaum, L. S. *Adv. Chem. Phys.* **1981**, *57*, 59−246.

(29) Fischer, G.; Cao, X. *J. Phys. Chem. A* **1999**, *103*, 3726−3731.

(30) Schaftenaar, G.; Noordik, J. H. *J. Comput.-Aided Mol. Des.* **2000**, *14*, 123−134.

(31) Bartlett, R. J.; Musial, M. *Rev. Mod. Phys.* **2007**, *79*, 291−352.

(32) Arulmozhiraja, S.; Ehara, M.; Nakatsuji, H. *J. Chem. Phys*. **2007**, *126*, 044306/1−044306/10.

(33) Limão-Vieira, P.; Eden, S.; Kendall, P. A.; Mason, N. J.; Hoffmann, S. V. *Chem. Phys. Lett*. **2002**, *364*, 535−541.

(34) *Chemical Kinetics and Photochemical Data for Use in Stratospheric Modeling*, Evaluation Number 12; JPL Publication 97-4; NASA, Jet Propulsion Laboratory: Pasadena, CA, 1997.

(35) Harris, W. C.; Longshore, C. T. *J. Mol. Struct*. **1973**, *16*, 187−204.